11th World Congress on Computational Mechanics (WCCM XI)
5th European Conference on Computational Mechanics (ECCM V)
6th European Conference on Computational Fluid Dynamics (ECFD VI)
E. Oñate, J. Oliver and A. Huerta (Eds)

MODELLING OF BALL BEARING LOADING BY DEM FOR ELECTROMECHANICAL COUPLING

C. MACHADO*, M. GUESSASMA* AND E. BELLENGER*

* Laboratoire des Technologies Innovantes (LTI) EA 3899
Université de Picardie Jules Verne
48 rue d'Ostende, 02100 Saint-Quentin
e-mail: charles.machado@u-picardie.fr

Key words: bearing loading, DEM, electrical measurement

Abstract. Rolling bearings are one of the most important and frequently encountered components in domestic and industrial rotating machineries. Statistical studies show that these bearings are considered as critical mechanical components which represent between 40% and 50% of malfunction in rotating machineries. This project represents a straight continuation of the research activities of the LTI and which helped to simulate and understand the electrical response of multi-contact systems [1]. In order to make further progress in the electromechanical modelling, the electrical transfer model is applied to the case of bearing operation [2]. An elastic 2D modelling by discrete elements [3] reproduces the dynamic bearing and the mechanical behaviour. A realistic load is applied to the bearing [5] and affects the electrical measurement. This study proposes an original method of measuring electrical resistance on the bearings to detect malfunctions (defects or unusual load). Each rolling element is a local electrical resistance determined by our model depending on the local loading. Indeed, while many studies have been conducted on monitoring bearing defects by analyzing vibration signals, the use of localized electrical measurements on bearings is a promising approach, not yet exploited. One of our objectives is to investigate the sensitivity of the electrical measurement due to the variation of mechanical loading.

1 INTRODUCTION

In order to ensure the industrial systems availability and the safety of goods and persons, the monitoring and diagnosis of bearing defects have to be considered with prime importance and the challenges in terms of productivity are non-negligible. Thus, defect detection in rolling element bearings has led to extensive research. Different experimental methods have been proposed for detection and diagnosis of bearing defects which may be broadly classified as vibration and acoustic measurements, temperature measurements,

defect signatures in the stator current motors, wear debris and lubricant analysis. Among these, vibration measurements are the most widely used. Knowledge of the state of load bearing is particularly important but in practice, it is difficult to determine the loading bearing accurately. An electric measurement is proposed to assist in determining the loading [2]. This unconventional approach attempts to measure the electrical resistance of the ball bearing in operation. The signature obtained includes indicators of the state of bearing load but also of the presence of possible defects, whether geometric or related to improper installation. Although, the presence of an electric current through the ball bearing is ordinary harmful, in this work the current densities required to perform a relevant experimental measurement are low to cause damage [9, 10]. From an experimental point of view, this technique could be advantageous at low speed when the lubrication regime allows the steel-steel contact. In these speed ranges (<100 revolutions/min), the conventional analysis techniques are difficult to implement.

2 Discrete modelling of a ball bearing

The ball bearing could be seen as a multi-contact system. The rolling elements and the cage are considered as discrete elements represented by sheres. Each discrete element is subjected to mechanical forces. The Non-Smooth Contact Dynamics formulation was first used in previous work [1, 2]. This approach was proved very restrictive when a realistic loading was considered because the particles are smooth. In this paper, we used the elastic Discrete Element Method (DEM), developed by Cundall and Strack [3]. The spherical particles are rigid and the interactions are governed by analogies with dumped springs.

2.1 General mechanical modelling

By using the Discrete Element Method, the contact points of the particles are described by contact models such as the elastic force displacement laws, the Coulomb friction and the viscous damping. The principle of the calculation is based on dynamic considerations. If the contact is detected ($\delta_n = R_{ij} - R_i - R_j < 0$), the springs are activated, here δ_n denotes the normal overlap, as suggested by figure (1). The equivalent model of the contact is given by figure (2). In figure 2, 5 parameters are introduced, K_n represents the normal

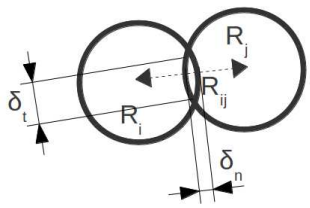

Figure 1: Description of the overlap between the particles

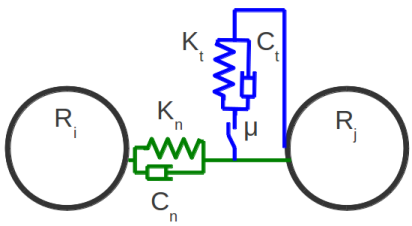

Figure 2: Contact modeling

stiffness and K_t represents the tangential stiffness. Stiffnesses are not sufficient to describe

the contact. To dissipate energy and move towards a steady state system, dampers are introduced in the normal direction, C_n and in the tangential direction, C_t. μ is a friction coefficient. The force F_i between particles includes the inter-particle interaction forces and the external forces.

$$\vec{F_i} = \sum_{j \neq i} \vec{F_{ij}} + \vec{F_{ext,i}} \tag{1}$$

$\vec{F_{ij}}$ is the force exerted by particle j to particle i. $\vec{F_{ext,i}}$ are the external forces on particle i (gravity, loading, ...). The contact force $\vec{F_{ij}}$ depends on the model chosen. From figure (2), this model included a normal component and a tangential component. $\vec{F_{ij}}$ is then decomposed as follow :

$$\vec{F_{ij}} = F_n \vec{n} + F_t \vec{t} \tag{2}$$

F_n is the contact force in the normal direction and F_t is the contact force in the tangential direction.

$$\begin{cases} F_n = K_n \times \delta_n + C_n \times \vec{v}.\vec{n} \\ F_t = K_t \times \delta_t + C_t \times \vec{v}.\vec{t} \end{cases} \tag{3}$$

where $\vec{v}$ is the relative velocity of the contact point between particles. δ_t can be approximated by the expression : $\delta_t = \vec{v}.\vec{t}\Delta_t$, with Δ_t is the time step.
F_t is a candidate force because the slider μ, due to dry friction is considered. Coulomb's friction law is written as follow and determines whether the contact is slipping or sliding :

$$F_t = -min(F_t, \mu F_n) \tag{4}$$

Usually, if K_n is determined with a model or with experimentation, the other parameters are fixed as follows :

$$\begin{cases} C_n = C_t = 2\sqrt{K_{n,t} \times m^*} \\ \frac{K_t}{K_n} \in [\frac{2}{3}, 1] \end{cases} \tag{5}$$

The viscous damping force is set critical ($2\sqrt{K_n \times m^*}$). m^* is the reduced mass. According to the Hertzian contact, the ratio $\frac{K_t}{K_n}$ can vary between $\frac{2}{3}$ and 1. Cundall and Strack [3] showed that the results do not depend on this ratio and other authors showed that C_n could be considered equal to C_t. The harmonic behaviour of linear model with constant parameters is well known but it is not sufficient in the context of our study. In our simulation of the ball bearing, the role of interactions at the contact plays an important role in the distribution of efforts. The non-linear interaction named the Hertz's law is introduced. The expressions of normal and tangential contact equivalent stiffness are directly related to the physical characteristics and dimensions of particles in contact in the relations established by Mindlin and Deresiewicz [13].

$$K_n^H = \frac{4G\sqrt{R_{eq}}}{3(1-\nu)}\sqrt{\delta_n} \tag{6}$$

and for no slip solution [4], the tangential stiffness is given by :

$$K_t^H = \frac{2(3R_{eq}G^2(1-\nu))^{1/3}}{2-\nu} \mid F_n \mid^{1/3} \tag{7}$$

where G is the shear modulus ($\frac{E}{2(1+\nu)}$) while E, the Young's modulus and ν is the Poisson's ratio. The expression of the normal force becomes:

$$F_n = K_n^H \times \delta_n + C_n \times \vec{v}.\vec{n} = \frac{4G\sqrt{R_{eq}}}{3(1-\nu)} \times \delta_n^{3/2} + 2\sqrt{K_n \times m^*} \times \vec{v}.\vec{n} \tag{8}$$

This type of non-linear model influences the response of the system. The contact force network is more realistic but the time step must be taken lower than linear model. The springs are related to the material properties and to the overlap δ_n.
The Hertz's stiffness could be determined as follow :

$$K_n = \frac{\partial F_n}{\partial \delta_n} = \frac{3}{2} K_n^H \tag{9}$$

Harris [5, 6] offers a similar normal model stiffness, derived from the Hertz's theory. The determination of the local stiffness is made by the radii of curvature $\sum \rho$ and introduces a dimensionless number δ^* related to the deformation. For a ball-steel raceway contact, the local normal stiffness is given by :

$$K_n^r = 2.15 \times 10^5 \sum \rho^{-1/2} (\delta^*)^{-3/2} \tag{10}$$

And the load-deflection relationship is given, without dumping, by :

$$F_n = K_n^r \delta_n^{3/2} \tag{11}$$

The following results are obtained using the Hertz's theory. Stiffnesses used are given by the expressions (6) and (7), the damping is critical.

2.2 Mechanical modelling of the ball bearing

A ball bearing is a particular type of multibody systems. Contacts in the ball bearings are not only of type ball/ball. The radii of the rings give a concave contact. The equivalent radii R_{eq} in expressions (6) and (7) should be calculated with the curvature of the rings. Quantities relating to loading of the bearing are introduced. The concept of preload/clearance will be taken into account, in our simulation. A deep groove ball bearing (SKF 6208) is modelled by using MULTICOR software [7], using the DEM. The 2D discrete model is composed of 2 rings and 13 balls. The cage of the ball bearing which ensures a constant interval between balls is modelled by 13 small balls. These balls are constrained by two boundaries in order to maintain them at the same distance from the

outer and inner races. The rolling elements and rings are made of steel. The modulus of elasticity of the steel is $E_b = 203$ GPa and its Poisson ratio is $\nu_b = 0.3$. The elements of the cage are made of polyamide, with a modulus of elasticity $E_c = 3$ GPA and a Poisson ratio $\nu_c = 0.3$. Only contacts between rolling elements and raceways have a non-zero friction coefficient ($\mu = 0.15$). The other contacts are considered purely slippery.

R_{out}	R_{inn}	R^c_{out}	R^c_{inn}	R_b	R_c
36.60 mm	24.00 mm	6.65 mm	6.55 mm	6.30 mm	1.00 mm

Table 1: Geometrical characteristics of the ball bearing

where, R_{out} is the outer ring race radius with R^c_{out}, the associated curvature radius. R_{inn} is the inner ring race radius with R^c_{inn}, the associated curvature radius. R_b is the rolling ball radius and R_c is the ball cage radius. In a deep groove radial bearing, the radius of the deep groove (curvature radius figure (4)) is always larger than the ball [11, 12] :

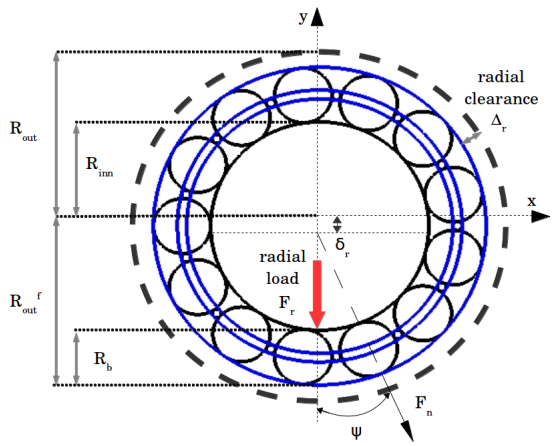

Figure 3: Characteristic dimensions of the ball bearing

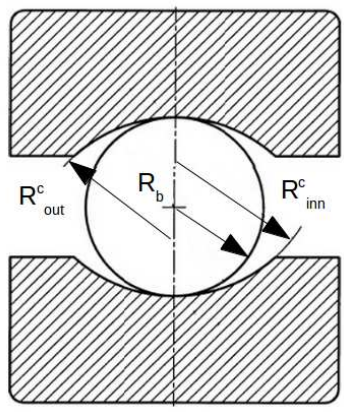

Figure 4: Compliance of the bearing rings

The simulations are conducted for different radial loads F_r. The preload and/or the clearance Δ_r is adjustable, as detailed in figure (3). The ball bearing loading is characterized by the loading factor ϵ.
Several concepts are introduced before rotating and because of the geometry of the ball bearing, the calculation of the necessary equivalent quantities to equations (6) and (7) is done as follows :

Contact	ball/cage	ball/inner raceway	ball/outer raceway	cage/cage
G	$\frac{G_b+G_c}{2}$	G_b	G_b	G_c
m^*	$\frac{m_i m_j}{m_i+m_j}$	m_i	m_i	m_i
R_{eq}	$\frac{r_i r_j}{r_i+r_j}$	r'_{inn}	r'_{out}	r_i

Table 2: Equivalent quantities depending on the type of contact

G_b and G_c respectively denote the shear modulus of steel and polyamide. m_i or m_j is the mass of the considered ball (cage or rolling element), with r_i and r_j are the associated radii.
The equivalent radius r'_{inn} is given by :

$$\left\{ \begin{array}{l} r'_{inn} = \frac{r_1 r_2}{r_1+r_2} \\ \alpha_{inn} = \frac{r_2}{r_1} \end{array} \right. \quad with \quad \left\{ \begin{array}{l} r_1 = \left(\frac{1}{R_b} + \frac{1}{R_{inn}}\right)^{-1} \\ r_2 = \left(\frac{1}{R_b} - \frac{1}{R^c_{inn}}\right)^{-1} \end{array} \right. \tag{12}$$

And the equivalent radius r'_{out} is given by :

$$\left\{ \begin{array}{l} r'_{out} = \frac{r_1 r_2}{r_1+r_2} \\ \alpha_{out} = \frac{r_2}{r_1} \end{array} \right. \quad with \quad \left\{ \begin{array}{l} r_1 = \left(\frac{1}{R_b} - \frac{1}{R_{out}}\right)^{-1} \\ r_2 = \left(\frac{1}{R_b} - \frac{1}{R^c_{out}}\right)^{-1} \end{array} \right. \tag{13}$$

α_{inn} and α_{out} are respectively the inner radius ratio and the outer radius ratio. These values are used to describe the ellipticity of the contact.

2.2.1 Clearance Δ_r

To adjust the radial clearance Δ_r, the radius of the outer race is gradually adjusted, compared to R_{out} [6]. In the simulation, the first calculation step will be dedicated to adjust the preload (or clearance). The final outer race radius is given by R^f_{out} and Δ_r is given by the difference between final radius R^f_{out} and initial radius R_{out} (given for $\Delta_r = 0$ in table 1):

$$\Delta_r = R^f_{out} - R_{out} \tag{14}$$

If $\Delta_r > 0$, a clearance is considered. $\Delta_r < 0$ is associated to a preload and the outer ring compress the system. Figure 3 shows this procedure.

2.2.2 Radial loading F_r

The radial loading F_r is considered as an external force and applied on the inner race according to the vertical direction $\vec{j}$, like the gravity (see figure 3). The F_r intensity is selected as a fraction of the basic dynamic bearing load C_r (for a 6208, NSK gives

$C_r = 29100N$ and SKF gives $C_r = 32500N$). The application of the force F_r causes a displacement of the center of the inner ring where δ_r is considered as the ring radial shift. The load parameter ϵ describes the state load of the ball bearing.

$$\epsilon = \frac{1}{2}\left(1 - \frac{\Delta_r}{\delta_r}\right) \tag{15}$$

These considerations, summarized by ϵ allow to load the desired number of rolling member and the remaining rolling elements can lose contact. For example, a load parameter $\epsilon = 0.5$ means $\Delta_r = 0$. F_r is distributed over half the rolling elements. A limit loading angle $\psi_l \pm 90$ is defined, beyond this angle, the rolling elements do not participate in the distribution of radial load.
Once the radial clearance Δ_r is applied and the radial load F_r is considered, the ball bearing will be gradually put in rotation. The inner ring rotates together with the shaft at an angular speed ω . The inner ring begins to rotate following a sinusoidal profile and then stabilizes at its threshold value ω.

3 Electromechanical modelling

Generally, the electrical transfer in multi-contact systems depends on the intrinsic mechanical and electrical properties of materials, the number and shape of particles and the contact number [1, 2]. Electrical response depends also on the mechanical loading applied to the ball bearing. In this study, we assume that the medium temperature is constant, the oxide layer on the surface of particles and the lubricant effects are not taken into account. The effect of roughness is neglected. The contact is perfect and the electrical transfer is described by a linear Ohm law. The formulation of the electrical problem is based on the contact force network of a multi-contact system. The main idea is to use the first Kirchhoff law and the Ohms law to build the problem to solve. The electrical potentials at each contact point are the unknowns of the electrical problem.
The electrical conductance between two contact surfaces S_i and S_j (contact surfaces at contact points i and j respectively) located on the surface of a homogeneous spherical particle k is given by :

$$C_{ij}^k = \frac{1}{R_{ij}^k} = \frac{\gamma S_i S_j}{2V_b}(1 - cos\theta) \tag{16}$$

where γ is the electrical conductivity of steel ($\gamma = 5.8 \times 10^7 S.m^{-1}$), V_b is the volume of the particle (rolling element), θ is the angle formed by the points i and j. The coupling between the mechanical and electrical computation is carried out by Hertz's theory. The element of the cage are insulating therefore only the rolling elements are involved in current transfer. In the ball bearings context, the ball-races contact surface is elliptical. The exact solution for the ellipsoid radii is quite complex. Hamroch and Brewe [11] suggested an approximate solution based on elliptical integrals. Each elliptical contact area is charaterized by its semi-major axis a and its semi minor axis b. The ellipticity parameter $k = \frac{b}{a}$

is given by the following approximation (for ball/inner race contact):

$$k \approx \alpha^{2/\pi} \tag{17}$$

α is given by expression (12). A dimensionless variable $\chi \approx 1 + \frac{q}{\alpha}$, with $q = \frac{\pi}{2} - 1$ is used to approximate the solution of the ellipsoid radii :
The ellipsoid radii a and b can now be calculated :

$$\begin{cases} a = \left(\frac{6\chi F_n R_{eq}}{\pi k E_{eq}}\right)^{1/3} \\ b = \left(\frac{6k^2\chi F_n R_{eq}}{\pi E_{eq}}\right)^{1/3} \end{cases} \tag{18}$$

where F_n is the normal contact force at the contact point. E_{eq} denotes the equivalent elastic modulus given by formula $E_{eq} = \frac{E_b}{1-\nu_b^2}$ (given in 2.2). The elliptical area is given by $S = \pi ab$. At time t, if a rolling element is in contact with the inner and the outer rings,

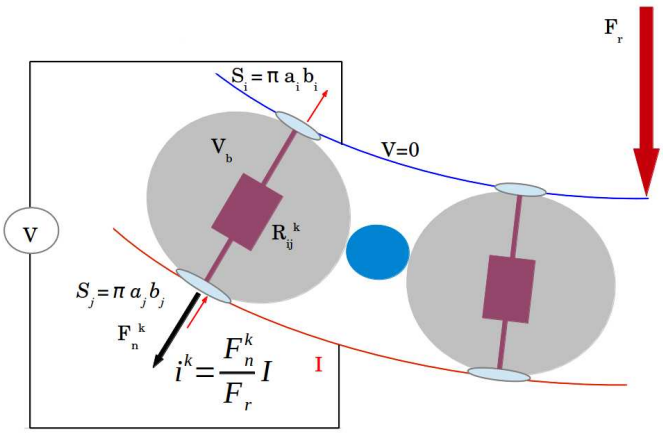

Figure 5: Illustration of electrical transfer in a rolling element

it contributes to the overall resistance of ball bearing. The angle θ is π.
A low electric current I is injected into the outer ring(race) and distributed according to the local loading, as illustrated in figure (5). Each ball/inner race contact are at zero potential. The current conservation is ensured between the rings. The combination of electrical resistors in parallel gives the overall resistance. From an experimental point of view, it seems that a current density greater than 0.1 A/mm^2 harms raceways [8, 9].

4 Simulation results

The proposed results are obtained for a fixed rotation speed ($\omega = 500 rad/s$) and the time step is $\Delta t = 10^{-7} s$. The first steps of the calculations are dedicated to load settings (Δ_r, F_r and ω). A parametric analysis is proposed. The load parameter ϵ is changed by F_r or by Δ_r and the electrical response is affected.

4.1 Electrical resistance according to radial load

Different radial loads, chosen as a fraction of the basic dynamic bearing loading C_r, are applied to ball bearings. There is no clearance ($\Delta_r = 0$) so the load parameter ϵ is set at 0.5, as suggested by figure (6). The percentage of rolling elements involved in the distribution of radial load is 50 % corresponding to 6.5 rolling elements.

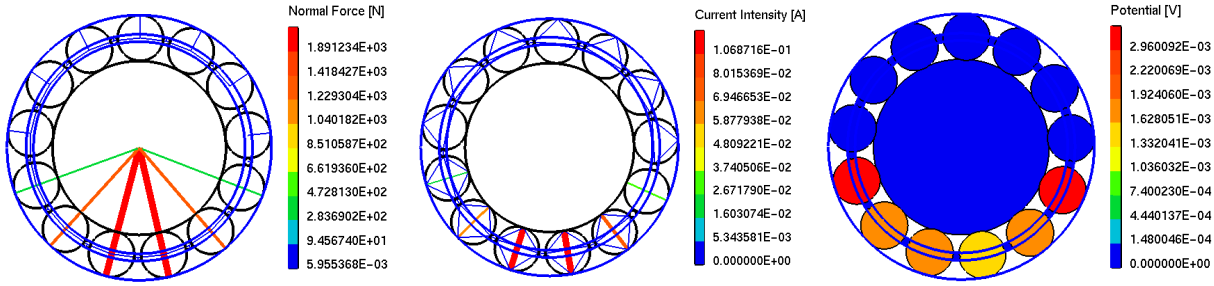

(a) (b) (c)

Figure 6: (a)Normal force (b)Electrical current and (c)Electrical potential, for $F_r = 5820N$ with $\epsilon = 0.5$

Figure 6(a) shows, at given time, how the radial load F_r is distributed within the ball bearing. The electric current follows this force distribution (figure 6(b)). The most loaded rolling element (close to $\psi = 0$ because $\vec{F_r} = -F_r\vec{j}$) allows to pass the most of electrical current. The electric potential given by figure 6(c) shows that only the loaded rolling elements are involved in electrical transfer. The insulating cage elements (in blue) block the electrical transfer between the rolling elements. The upper bearing zone is not concerned by the electric transfer for this type of loading. Each rolling element requested in the electrical transfer offers a different electrical resistance, based on the model (16). The overall electrical resistance is obtained by the parallel combination.
To understand what happens at the local level, a ball is followed during a rolling round. This ball receives a part of the radial load F_r, depending on its position, in the load zone ψ_l. The normal contact force $F_n = \sqrt{F_{n,x}^2 + F_{n,y}^2}$ between the ball and the outer race is represented in figure (7), for several radial load.
F_n includes the part of the radial load supported by the ball, the centrifugal effect and the mass of the ball. Each radial load gives the same distribution (same form during a rolling round). Profiles are symmetrical to the axis of radial loading F_r. The main difference between the graphs is the maximum load carried by the ball, resulting in the vertical direction ($F_r = -F_r\vec{j}$). At each radial load is associated the electrical resistance according to time, given in figure (8). As expected, when the radial force F_r increases, the electrical resistance decreases but this dependency is no linear according to Hertz's theory.

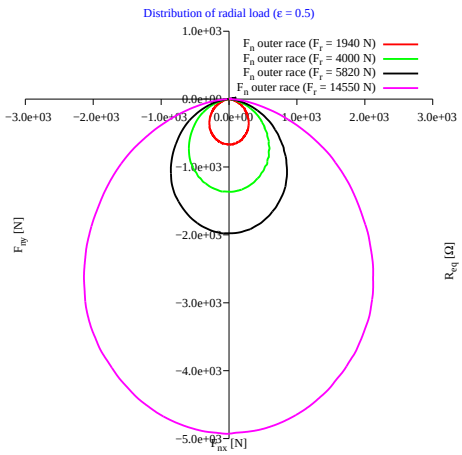

Figure 7: Radial load distribution of a ball on a rolling round (ω = 500 rad/s and $\epsilon = 0.5$)

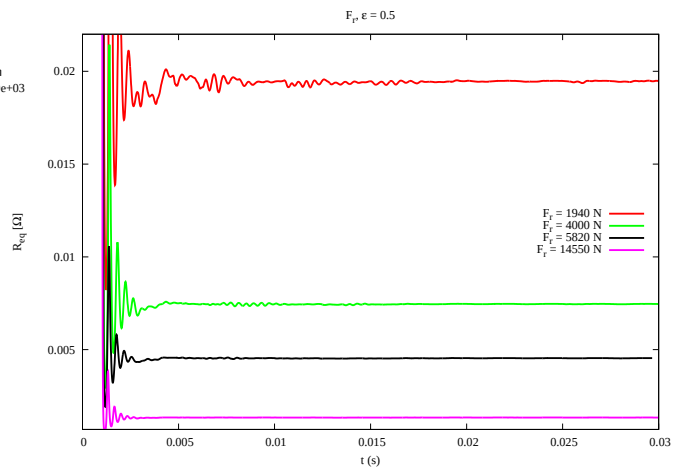

Figure 8: Electrical resistance versus time with different radial loads ($\omega = 500$ rad/s and $\epsilon = 0.5$)

4.2 Electrical resistance according to load parameter

The radial load F_r is fixed at 5820 N. The load parameter ϵ is modified by using a different clearances ($\Delta_r < 0$, $\Delta_r = 0$ and $\Delta_r > 0$). Figure (9) gives an example of load distribution with $\epsilon = 0.3$. The average number of loaded rolling elements is less than 50%.

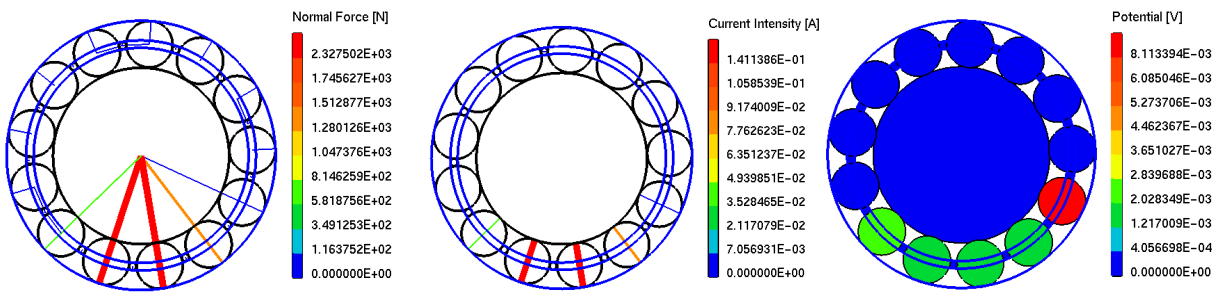

(a) (b) (c)

Figure 9: (a)Normal force (b)Electrical current and (c)Electrical potential, for $F_r = 5820N$with $\epsilon = 0.3$

The observations are similar to those given in the previous paragraph. The distribution of radial load depends on the load parameter ϵ. A ball is followed during a rolling round, for several load parameters with $F_r = 5820$ N. The normal contact force F_n between the ball and the outer race is represented in figure (10). A consequence is that the followed ball is less loaded. The ball does not lose contact during rolling round. At each ϵ is associated the electrical resistance according to time, figure (11). The first moments, until $0.005s$ is a damping phase, the system responds to the imposed constant loading F_r.

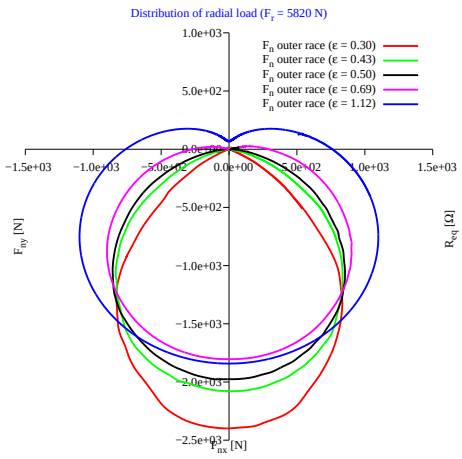

Figure 10: Radial load distribution of a ball on a rolling round

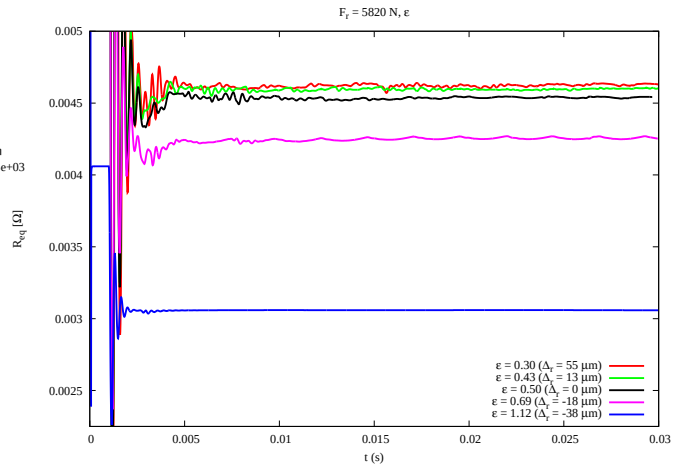

Figure 11: Electrical resistance versus time with different load parameters ($\omega = 500$ rad/s and $F_r = 5820$ N)

Observing the graph (11) shows that when ϵ increases, the electrical resistance decreases. The preload Δ_r ($\Delta_r < 0$) introduces an additional loading. Moreover, it seems that a low load parameter causes noisy resistance. This is probably due to a large clearance. This effect is less noticeable in figure (8).

5 Conclusion

The description of the dynamic behavior of ball bearings using analogies with stiffness gives good results with Hertz's model. Load distribution of the ball bearing is determined by the choice of the mechanical model. An electrical measurement is proposed to check the loading effect of the mechanical types loading. The electrical sensitivity of this measurement allows to distinguish different type of loadings (amplitudes, load parameters). Subsequently, abnormal loads, misalignments and defects will be imposed on ball bearings and their electrical signatures will be analysed. For now, the electrical model considers a dry contact but it can be planned to complete this model by taking into account the effect of lubricant with the theory of elastohydrodynamic lubrication [10] while the lubricant acts as a capacitor. Similarly, the mechanical model is based on a no slip approximation but other models include the stick-slip. In a future work, simulation results will be compare with experimental measurements. The harmlessness of this measure will be highlighted.

Acknowledgements : *This study has been carried out under project SIGNATELEC (2012-2015). Thanks to the "Région de Picardie" for its financial support*

REFERENCES

[1] Bourbatache K., Guessasma M., Bellenger E., Bourny V. and Tekaya A., *Discrete modeling of electrical transfer in multi-contact systems*, Granular Matter, vol 14(1), 1-10, 2012.

[2] Bourbatache K., Guessasma M., Bellenger E., Bourny V., Fortin J., *DEM ball bearing model and defect diagnosis by electrical measurement*, Mechanical Systems and Signal Processing, vol 41(1-2), 98-112, 2013.

[3] Cundall PA, Strack ODL. *A discrete numerical model for granular assemblies.* Geotechnique,vol 29(1), 47-65, 1979.

[4] Tsuji Y., Tanaka T., and Ishida T., *Lagrangian numerical simulation of plug flow of cohesionless particles in a horizontal pipe.* Powder Technology, vol 71, 239-250, 1992.

[5] Harris T., *Rolling Bearing Analysis*, Wiley and Sons, 2001.

[6] Harris T., *How to Compute the Effects of Preloaded Bearings*, Prod. Eng., vol 19, 84-93, 1965.

[7] Fortin J., Millet O., De Saxcé G., Numerical simulation of granular materials by an improved discrete element method, Int. J. Numer. Methods Eng., vol 62, 639-663, 2004.

[8] Muetze A., *Currents in Inverter-Fed AC-Motors*, Thesis, Darmstadt, 2004.

[9] Stack J.R., Habetler T.G.,Harley R.G., *Experimentally generating faults in rolling element bearings via shaft current*, IEEE Transactions on Industry Applications, vol 41(1),25-29, 2005.

[10] Busse D.F., Erdman J.M, Kerkman R.J.,Schlegel D.W., Skibinski G.L., *The effects of PWM voltage source inverters on the mechanical performance of rolling bearings*, IEEE Transactions on Industry Applications, vol 33(2), 567-576, 1997.

[11] Hamrock B.J., Anderson W.J., *Rolling-Element Bearings*, NASA, RP1105/REV1, 1983.

[12] Hamrock B.J., Anderson W.J., *Analysis of an Arched Outer Race Ball Bearing Considering Centrifugal Forces*, ASME Jour. of Lub. Technol., vol 95, no.3, 265-276, 1973.

[13] Mindlin R.D., Deresiewicz H., *Elastic Spheres in Contact under Varying Oblique Force.* ASME Journal of Applied Mechanics, vol 20, 327-344, 1953.

[14] Mindlin R.D., *Compliance of Elastic Bodies in Contact.* ASME, Journal of Applied Mechanics, vol 16, 259-268, 1949.